Electrochimica Acta 388 (2021) 138613

Contents lists available at ScienceDirect

Electrochimica Acta

journal homepage: www.elsevier.com/locate/electacta

Improving the onset potential and Tafel slope determination of earth-abundant water oxidation electrocatalysts

Roger Sanchis-Gual[a,1], Alvaro Seijas-Da Silva[a,1], Marc Coronado-Puchau[a], Toribio F. Otero[b,*], Gonzalo Abellán[a,*], Eugenio Coronado[a]

[a] Instituto de Ciencia Molecular, Universidad de Valencia, Catedrático José Beltrán 2, 46980 Paterna, Spain
[b] Centre for Electrochemistry and Intelligent Materials (CEMI), Universidad Politécnica de Cartagena, Paseo Alfonso XIII, E-30203 Cartagena, Murcia, Spain

ARTICLE INFO

Article history:
Received 5 May 2021
Accepted 8 May 2021
Available online 15 May 2021

Keywords:
Onset potential
Coulovoltammetry
Oxygen evolution reaction
Layered hydroxides
Prussian blue analgue

ABSTRACT

To date, a plethora of electrocatalysts for the Oxygen Evolution Reaction (OER) have been proposed. For evaluating their electrocatalytic behavior the determination of the onset potential in each studied electrolyte is a key parameter. Nevertheless, this evaluation becomes particularly problematic for first-transition metal catalysts as well as by the use of electroactive collectors (*e.g.* Ni foams) whose redox peaks overlap the onset potential. A usual solution to detect the onset potential requires the availability of *in-situ* mass spectrometric determination of the generated oxygen. In this work, we present fast and easier available cyclic voltammetry and coulovoltammetric responses to determine the onset potentials of three benchmark electrocatalysts: a layered double hydroxide, a Prussian blue analogue and a β-Layered hydroxide. Cyclic coulovoltammetric responses allow, as we demonstrate here, a quantitative separation in the same potential range of the charge consumed by reversible (redox) reactions and the charge consumed by the irreversible reaction: the oxygen release. Quantifying the irreversible charges (that correspond to the OER) for different anodic potential limits permits the unambiguous determination of both, the onset potential and the Tafel slope values without the catalyst redox contributions. As far as we know, this is the first time that this fast, available and cheap methodology has been applied for the OER determination. Thus, coulovoltammetry arises as a friendly and powerful tool for the investigation of electrocatalytic performances.

1. Introduction

Water oxidation, also known as Oxygen Evolution Reaction (OER), is considered as the energetic limiting reaction for water-splitting. It is a critical reaction for sustainable electrochemical fuel generation and energy storage with major applications including solar water-splitting devices, electrochemical CO_2 reduction, and metal–air batteries and fuel cells [1–3]. Nonetheless, this reaction gives rise to an important energetic efficiency loss in water-splitting systems due to both, its slow kinetics (low current density) and high overvoltage: the consumed energy is the charge consumed in a period of time multiplied by the overpotential. Good electrocatalysts are required to minimize the energetic requirements: a flow of very high currents at overpotential as low as possible. In this context, a plethora of electrocatalysts have been proposed including earth-abundant compounds in their composition [4–10]. Enormous efforts have been made to improve the electrochemical performance, stability and integration of such electrocatalysts [11–16]. One of the main problems in this field shows up when we try to compare the different electrochemical parameters of the proposed electrocatalysts. In fact, these concerns have been addressed many times by the scientific community [17–22], emerging a precise determination of both, the OER onset potential and the Tafel slope as the main problems. The onset potential is the highest (for cathodic reactions) or lowest (for anodic reactions such as the OER) potential values at which a reaction product is produced at a given electrode and defined conditions. As indicated above it is one of the key parameters, next to the Tafel slope, for evaluating the catalytic energetic performance of any electrocata-

* Corresponding authors.
E-mail addresses: toribio.fotero@upct.es (T.F. Otero), gonzalo.abellan@uv.es (G. Abellán).
[1] Author Contributions: The manuscript was written through contributions of all authors. / All authors have given approval to the final version of the manuscript.These authors contributed equally.

https://doi.org/10.1016/j.electacta.2021.138613

lyst and thus, it must be extracted with care. The onset and Tafel slope determination get even more complicated when the electrocatalysts include first-transition metals and/or the collector is electroactive (such as nickel foam). In both cases, reversible oxidation/reduction reactions to give/reduce oxides and hydroxides usually overlap (occur in the same potential range as) the onset potential. This makes it difficult to correctly estimate the Tafel slope. In addition, the overpotential required to flow a current density of 10 mA cm^{-2} is used as another parameter to compare different electrocatalysts. However, the presence of redox peaks can also contribute to this current density that, additionally, is extremely dependent on the calculation of the area of the working electrode, making this comparison difficult and imprecise [18,23]. To date, the typical solution to detect the onset potential involves the usage of a mass spectrometry equipment that detects the *in-situ* oxygen production [23–25]. Nevertheless this technique is only available in few laboratories.

In order to overcome these limitations, we propose here determining the O_2 production of three different and well-known electrocatalysts (NiFe-LDH, CoFe-PBA and β-$Co(OH)_2$) during the redox process by means of the coulovoltammetric (QV) responses (which are attained by integrated voltammetry) to the application of potential cycles [26,27]. The proposed methodology, cyclic voltammetry (CV), is very common in laboratories devoted to the development of new OER electrocatalysts. The breaking point proposed here is using, instead of the classical voltammetric (current/potential) responses, the less usual coulovoltammetric (QV, charge/potential) responses.

2. Experimental

2.1. Reagents

All chemical reagents were purchased and used without further purification. Potassium ferricyanide, cobalt (II) chloride hexahydrate, nickel (II) chloride hexahydrate, iron (III) chloride hexahydrate, triethanolamine (TEA), hexamethylenetetramine (HMT), sodium carbonate and potassium hydroxide (99.99%) were purchased from Sigma-Aldrich. Ethanol absolute (EtOH) was purchased from Panreac. Carbon black, acetylene 50% compressed, was obtained from Alfa Aesar (99.9%). The oxygen test was purchased from Merk (1.11107.0001). Milli-Q water was obtained from a Millipore Milli-Q equipment.

2.2. Physical characterization

Attenuated total reflectance Fourier-transform infrared (ATR-FTIR): spectra were collected in an Agilent Cary 630 FTIR spectrometer in the 4000−400 cm^{-1} range in absence of KBr pellets. Energy Dispersive X-Ray (EDX) spectroscopy: EDX studies were performed on a HitachiS-4800 microscope at an accelerating voltage of 20 kV without metallization process. Elemental analysis (EA): Carbon and hydrogen contents were determined by microanalytical procedures by using an LECO CHNS-932. Inductively Coupled-Plasma Mass Spectrometry (ICP-MS): The ICP-MS analysis were conducted at the Universidad de Valencia (Sección de Espectrometría Atómica y Molecular). Samples were digested in an acid medium at 220 °C using a microwave oven. Transmission Electron Microscopy (TEM): TEM studies were carried out on a JEOL JEM 1010 microscope operating at 100 kV. Samples were prepared by dropping suspensions on lacey formvar/carbon copper grids (300 mesh). X-Ray Powder Diffraction (XRPD): XRPD patterns were obtained with a PANalytical X'Pert diffractometer using the copper radiation (Cu-Ka = 1.54178 Å) in the 5–50 region.

2.3. Electrocatalysts synthesis

2.3.1. Layered Double Hydroxide (LDH) synthesis

The LDH of NiFe-CO_3 was obtained by anion exchange reaction from a NiFe-Cl. 200 mg of LDH NiFe-Cl was added to 100 mL of a water solution 0.2 M Na_2CO_3. Then the reaction was maintained for 24 h at room temperature and finally, the mixture was filtered, and the yellow powder was washed with H_2O and EtOH several times and dried during 24 h in vacuum.

The pristine LDH NiFe-Cl with Ni/Fe ratio of 3:1 was synthesized using a hydrothermal previous report by our group in Carrasco *et al.* [28]. Briefly, a 1:1 (v/v) ethanol/ water solution 20 mM of metal cations with a relation Ni/Fe 3:1 and 0.1 M of TEA was transferred to a Teflon-lined stainless steel autoclave. The autoclave was placed in a preheated oven at 120°C for 6 h. Finally, it was cooled to room temperature, and the final brown powder was filtered and washed with H_2O and EtOH several times and dried during 24 h in vacuum.

2.3.2. Prussian Blue Analogue (PBA) synthesis

The PBA of CoFe was synthesized at room temperature by adding, to 100 mL aqueous solution at 2 mL h^{-1} rate, aqueous solutions of $CoCl_2 \bullet 6H_2O$ (5.0 mM, 10 mL) and $K_3[Fe(CN)_6]$ (5.7 mM, 10 mL) were added simultaneously. After completion of the addition, the mixtures were stirred for half an hour before being centrifuged at 10000 rpm for 20 min. The supernatant was removed, and the powder was let dry under vacuum.

2.3.3. β-Layered hydroxide synthesis

The β-cobalt hydroxide was synthetized by a previous reported [29]. The synthesis was performed in a flask under an N_2 atmosphere protocol. In a typical procedure, $CoCl_2$,$6H_2O$ and HMT were dissolved in 1.5 L of a 9:1 mixture of deionized water and ethanol to give the final concentrations of 5 and 60 mM, respectively. The reaction solution was then heated at about 95°C under magnetic stirring. After being heated for about 5 h, a suspension containing pink particles is obtained. The solid product was filtered and washed with deionized water and anhydrous ethanol several times, and finally air-dried at room temperature.

2.3.4. Electrode preparation

For the electrochemical measurements, a mixture of the LDH or PBA or β-$Co(OH)_2$, acetylene black, and PTFE in ethanol in a mass ratio of 80:10:10 was prepared and deposited on a nickel foam electrode. The as-prepared electrode was dried for 2 h at 80°C. Each working electrode contained ~0.5 mg of the electrocatalyst and had a geometric surface area of ~2 cm^2. Thus, the electrode mass loading achieved was 0.25 mg cm^{-2}.

Modified LDH glassy carbon rotating disk electrode (GC RDE) was also prepared. An initial suspension was prepared by adding 25 μL of 5% Nafion solution to 5 mg of LDH powder and 2.5 mg of graphitized carbon and then dispersed in 1.25 mL of 1:1 (v/v) EtOH/H_2O and sonicated for 20 min. 5 μL of this dispersion were drop-casted onto a previously polished (sequentially with 1.0, 0.3, and 0.05 μm alumina powder) 3 mm diameter RDE and dried at room temperature for 30 min.

2.3.5. Electrochemical measurements

The electrochemical tests were performed in a typical three-electrode cell equipped with the modified Ni foam acting as the working electrode and a platinum wire as the counter electrode. As the reference electrode, a silver-silver chloride (versus Ag/AgCl (3 M KCl)) was used. All potentials were converted referring to the oxygen evolution overpotential. An Autolab PGSTAT 128N potentiostat/galvanostat was used to perform the electrochemical measurements. Oxygen Evolution Reaction measurements were carried out

at 5 mV s^{-1} in a previously N_2 purged 1 M KOH aqueous solution. The third cycle for each voltammetric experiment was analyzed (after observing the same response in the second and the third cycle). Prior to this, an activation process of the prepared electrode (consisting of 30 voltammetric cycles between -0.3 V and 0.25 V) at 50 mV s^{-1} in a 1 M KOH aqueous solution was performed. This activation process is carried out until the CV of the material is stable, ensuring the absence of new irreversible processes related to the material.

Chronoamperometric measurements were carried out at constant overpotentials of 0.15 and 0.2 V for NiFe-LDH, 0.10 and 0.15 V for CoFe-PBA and 0.125 and 0.175 V for β-$Co(OH)_2$, applied to the working electrode during 1 hour using 30 mL of 1M KOH aqueous solution for each experiment. Gamry 1010E potentiostat–galvanostat controlled by Gamry software was used to perform these experiments.

All electrochemical measurements were made ensuring that the meniscus that is generated around the electrode does not touch the alligator clips.

2.4. O_2 determination by Winkler titration

After chronoamperometry measurements, the pH of the resulting solution was adjusted to 6-8 by adding a N_2 purged H_2SO_4 0.5 M solution. O_2 concentration was determined using the oxygen test (1.11107.0001). Essentially, the O_2 concentration was determined after several reactions through iodometric titration.

In this sense, a basic aqueous solution of $MnCl_2$ and KI is added to the previous solution. Under alkaline conditions, the dissolved oxygen oxidizes Mn(II) to $MnO(OH)_2$, converting the dissolved gas to a solid. Afterwards, in a strongly acidic solution, the dissolved Mn reacts with iodide to form iodine that is titrated with thiosulfate by iodometric titration using starch as indicator. The initial O_2 concentration is thus determined from the consumed thiosulfate.

To compare the different samples correctly, the O_2 was determined after applying an overpotential for 1 h in 20.0 mL of a previously N_2 purged KOH 1 M solution in a sealed electrochemical cell.

3. Results and discussion

3.1. Coulovoltammetric (QV) response

QV responses, which are directly provided by the software available in electrochemical equipments, have been mainly used to detect energetic asymmetries between oxidation and reduction reactions as well as structural changes occurring during those reactions. Moreover, these can also be used to detect the presence of parallel irreversible reactions of some of the electrolyte components during the reversible oxidation/reduction reactions of the conducting polymer film [30,31]. Essentially, the QV cycle shows (Fig. 1) the evolution of the charge consumed by the material reactions in parallel to the voltammetric response to the applied potential cycle. The anodic branch includes the charge consumed to oxidize the material in combination with the irreversible OER, while the cathodic branch only includes the charge consumed to reduce the oxidized material. Accordingly, reversible and irreversible charges can be separated and quantified. Therefore, the charge corresponding to the OER (*i.e.* irreversible charge) as a function of different experimental variables can be attained and further analyzed. This technique is quite simple and shows up as a friendly and potential tool to explore the onset potential and the Tafel slope.

QV responses, when the software does not provide them directly, are obtained by integrating the voltammetric results. The

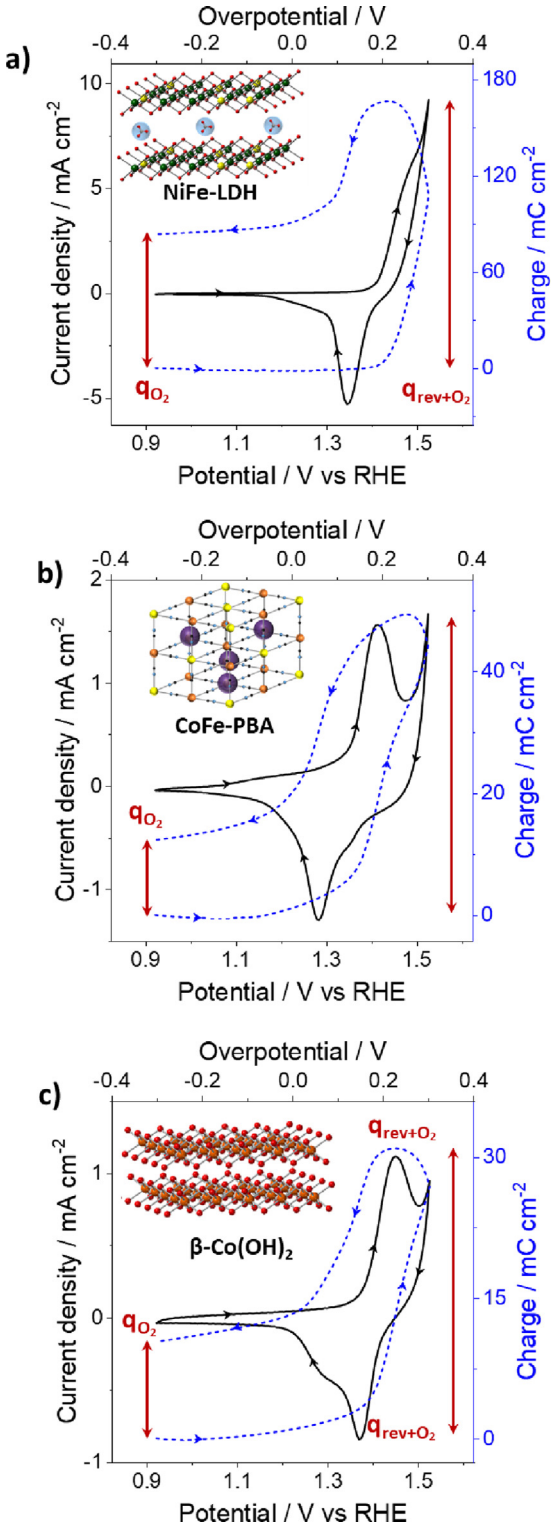

Fig. 1. Coulovoltammetric (QV) responses and parallel voltammetric (CV) responses for a) NiFe-LDH, b) CoFe-PBA and c) β-$Co(OH)_2$. All measurements were performed at 5 mV s^{-1} in a previously N_2 purged 1 M KOH aqueous solution. Overpotentials are calculated by subtracting the applied potential from the OER potential (E_{app} – E_{OER}).

charge density, C cm^{-2}, consumed by the reactions at each voltammetric time (q_t) is:

$$q_t = \int_0^t j(t)dt \quad (1)$$

where the integral is the area under the voltammetric response from the beginning of the reaction (j = 0, mA cm^{-2}, for any potential, or time because potential and time are linked by the potential sweep rate ν, mV s^{-1}, t (s) = V/ν, below the standard potential of the reaction).

Here, oxidation reactions lead to positive charge increments, while reduction reactions lead to negative charge increments. When the voltammetric response only involves reversible redox processes of the electrodic materials, the positive charge increment during the anodic potential sweep is equaled to the negative charge increment during the cathodic potential sweep giving closed QV loops. When an irreversible reaction (*e.g.* the oxygen evolution) overlaps the formation of reversible metal oxides during the anodic potential sweep, the charge consumed during this anodic sweep (formation of reversible metal oxides plus oxygen release) overcomes the charge consumed during the cathodic potential sweep (reduction of metal oxides) giving open QV loops. The charge difference between the beginning and the end of the open-loop gives the charge consumed by the irreversible OER. Hence, QV responses allow a good graphical separation, identification and quantification of the charges involved in reversible or irreversible reactions taking place in the same potential range.

3.2. Coulovoltammetric (QV) response for the electrocatalysts study

The utility and the interest of using QV to analyze electrocatalysis are illustrated here by studying three different electrocatalysts: a layered double hydroxide (NiFe-LDH), a Prussian blue Analogue (CoFe-PBA) and a β-layered hydroxide (β-$Co(OH)_2$) [28,29,32]. The full characterization of all the materials studied can be found in the Supporting Information (Figs. S1, S2 and S3, respectively).

Firstly, consecutive potential cycles were applied to NiFe-LDH, CoFe-PBA and β-$Co(OH)_2$ electrodes at 50 mV s^{-1} using Ni foam collectors as supporting metal electrode in a 1 M KOH aqueous solution previously purged by N_2 bubbling for 10 min under ambient temperature. Figure S4 shows the 30 initial voltammetric responses. After 15 consecutive potential cycles of electrocatalytic activation, the voltammetric and QV responses overlap getting stationary responses (Fig. 1). In this Figure, the reversible oxidation process of NiFe-LDH and cobalt-containing materials can be observed between 0.20–0.30 V (Fig. 1a) and 0.15–0.25 V (Fig. 1b), respectively [33,34]. These are typical CVs for first-transition metal electrocatalysts. Their integration gives, in all cases, open coulovoltammograms overlapped on the same Figure. We observe that the charge at the end of the cycle is shifted anodically with respect to the zero charge at the beginning of the potential cycle. This indicates that a good fraction of the charge consumed by oxidation reactions during the anodic potential sweep was not recovered by reversible reduction reactions during the cathodic potential sweep. This is indicative of the existence of an irreversible process related to the OER. The charge gradient between the initial and the final points of the QV cycle quantifies the charge consumed by the irreversible reaction in that potential range, q_{irrev}. The total QV charge density (charge at the QV maximum minus charge at the QV minimum) gives the total QV charge density, q_t. The difference gives the charge density involving reversible oxidation/reduction metal processes in the studied potential range, q_{rev}. As conclusion:

$$q_t = q_{irrev} + q_{rev} \quad (2)$$

or,

$$q_{irrev} = q_t - q_{rev} \quad (3)$$

Our goal is to determine the potential where the irreversible oxygen release (anodic reaction) starts. This irreversible charge is consumed here to produce oxygen by water splitting:

$$q_{irrev} = q_{O_2} \quad (4)$$

It is important to remark that the reported methodology can be applied as long as the redox processes are reversible, while the irreversible reaction corresponds to the OER. In this sense, activation cycles must be performed to get the same amount of material being oxidized/reduced in each voltammetric cycle and thus, minimize the irreversibility of the redox reaction (corrosion). On the other hand, this protocol would not be applicable in the cases where other irreversible reactions, non-related to the OER, which could persist after the activation process are still present (*e.g.* ammonia oxidation or formic acid oxidation).

Using CV and QV responses and maintaining the other experimental parameters constant, we can now explore larger cathodic potential limits to confirm the existence and persistence of an irreversible oxidation process, and to exclude non-completed reduction reactions (see Figure S5). In order to check that the electroactivity of each catalyst remains constant (without alteration of both, the position and the intensity of the redox peaks) voltammetric controls were performed on each material before and after the window potential widening (Figure S6).

3.3. Onset determination by QV response

Similar experiments were carried out fixing now the cathodic potential limit and varying the anodic potential limit (Figure S7). Both reversible and irreversible charge densities (*i.e.* q_{rev} and q_{O2}) rise for increasing anodic potential limits. That means that both processes coexist in the studied potential range. Thus, a higher reversible charge is consumed when the anodic potential limit increases indicating that more metal atoms are oxidized at increasing anodic potentials to form the electrocatalytic species and, as expected, higher irreversible charges are consumed in parallel by the oxygen production. Considering the reversible behavior of the metal reactions, q_{O2} can be easily extracted and analysed.

The charges consumed by the oxygen evolution during potential cycles performed up to different anodic potential limits are presented as points related to that potential limit, overlapped to a conventional CV in Fig. 2. In agreement with the previous *in-situ* experiment, the existence of q_{O2} during the redox process can be seen [18,23]. The O_2 formation starts at 0.2 V, 0.15 V and 0.175 V for NiFe-LDH, CoFe-PBA and β-$Co(OH)_2$ (insights from Figs. 2a, 2b and 2c), respectively. These values represent an unambiguous determination of their respective onset potential (Table 1). At this point, it is important to note that the cobalt-containing materials show lower onset potential than the benchmark electrocatalyst for OER (NiFe-LDH). However, these materials exhibit slower kinetics towards OER as can be noticed by comparing the current densities at rising overpotentials. Indeed, an irreversible charge density of 100 mC cm^{-2} is achieved at 0.30 V for LDH, while for the cobalt-based materials studied this is achieved above 0.35 V. This aspect

Table 1
Onset potential and Tafel slope obtained for earth-abundant electrocatalysts by using QVs (*i.e.* integrated voltammetry).

Electrocatalyst	Onset potential / V	Tafel slope / mV dec^{-1}
NiFe-LDH	0.200	62
CoFe-PBA	0.150	120
β-$Co(OH)_2$	0.175	137

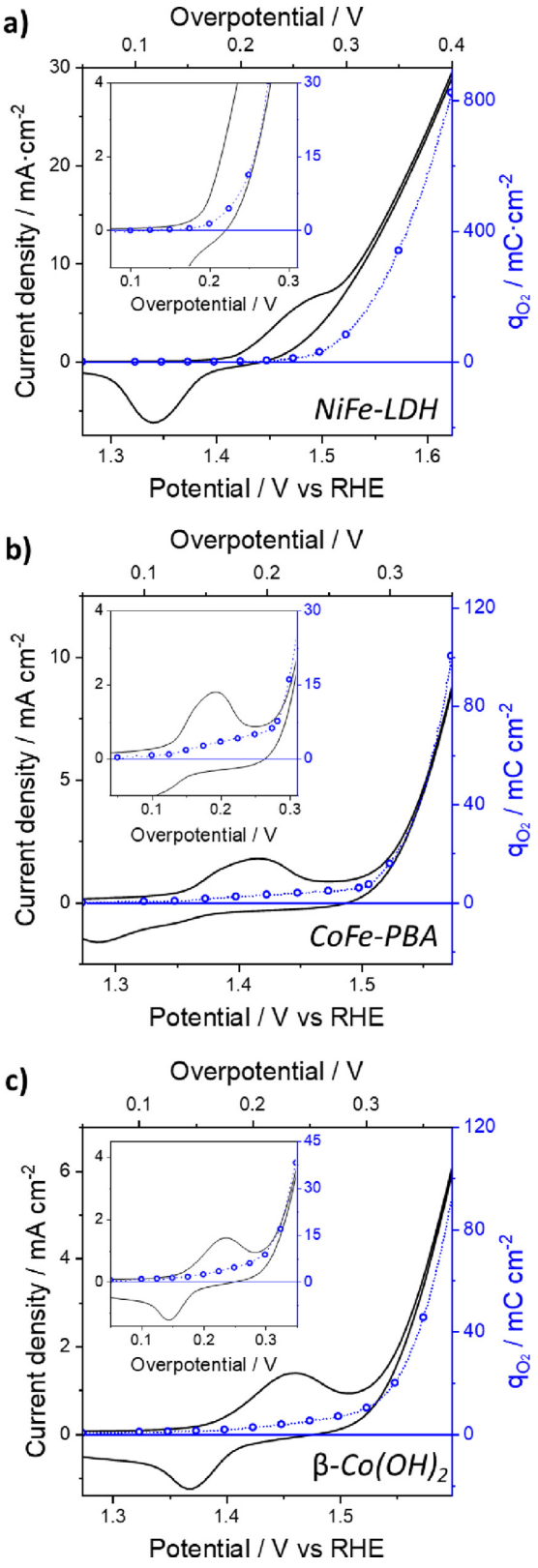

Fig. 2. Evolution of the irreversible charge (q_{O2}), blue points, in parallel to the voltammetric response full lines) to the cyclic voltammetry for a) NiFe-LDH, b) CoFe-PBA and c) β-Co(OH)$_2$. The CVs were performed at 5 mV s^{-1} in a previously N_2 purged 1 M KOH aqueous solution.

is a clear example that for the complete characterization of an electrocatalytic material a precise determination of both the onset and the Tafel slope is mandatory.

3.4. Tafel slope determination by QV response

Best practices related to the Tafel slope determination recommend the use of a rotating disk electrode in order to avoid the contribution of mass-transport. Moreover, the use of low scan rates ($\leq$ 5 mV s^{-1}) is indispensable to an accurate determination of Tafel slope [17,35]. Nevertheless, the conditions that are usually applied to characterize OER electrocatalysts do not involve forced convection. Indeed, the most common substrates (which have a strong influence on the electrocatalytical performance [36]) are Ni foam, Glassy Carbon, graphite paper and Ti mesh since they improve considerably the OER performance or they are more available compared to RDE [37–41]. Indistinctly, regarding the study of first transition electrocatalysts, the Tafel slopes are often estimated in the literature inside the redox potential window leading to inaccurate values and a huge dispersion between similar materials.

By taking advantage of QVs, Tafel slopes corresponding exclusively to the OER can be calculated by using the q_{O2} rather than using the current densities where redox and OER processes are overlapped (Fig. 3). The current density, j, and the consumed charge density at any overpotential are linked by Eq. 1. In this scenario, Tafel slopes of 62 mV dec^{-1}, 120 mV dec^{-1} and 137 mV dec^{-1} are calculated for the LDH, PBA and β-Co(OH)$_2$, respectively. Comparing these values with the ones obtained by representing the current density (*i.e.* including reversible and irreversible processes), we notice that at low overpotentials the Tafel slopes are underestimated due to the material redox reactions. In contrast, at high overpotentials, the values are overestimated because the reaction is under diffusion control. These results pinpoint QVs as an efficient and reliable technique to get a precise estimate of Tafel slopes, clearing out spurious information.

Therefore, the separation of reversible and irreversible contributions makes possible an accurate calculation of the Tafel slopes corresponding to OER. It is worth noting that now the separation of reversible and irreversible contributions facilitates a new approach for the calculation of this parameter corresponding to the OER. In view of these results, the estimated values of the Tafel slope for NiFe-LDH, CoFe-PBA and β-Co(OH)$_2$ are listed in Table 1.

Moreover, this methodology can be also employed to determine the onset potential and the Tafel slope of electrocatalysts measured in RDE when a redox peak overlaps the onset (Figure S8).

3.5. O_2 determination by Winkler titration

To corroborate the information extracted from the QV, the Winkler Method [42] was used to determine the presence of dissolved O_2 in the solution after applying a fixed overpotential near the estimated onset potential. To do so, chronoamperometries were performed at different overpotentials during 1 h (Figure S9) and the resulting O_2 dissolved in the aqueous solution was analyzed in triplicate. For all the electrocatalysts, the application of the overpotential indicated by QV as the onset gives rise to a constant current of around 10 μA cm^{-2}, which can be associated with the OER. In addition, lowering the applied voltages slightly by 0.05 V leads to current densities of almost 0. These facts were confirmed by measuring the dissolved O_2 concentration in the resulting solutions. Previously, to ascertain the precision of this determination, the dissolved O_2 was analyzed at different overpotentials, observing, as expected, a progressive increase of the produced O_2 with the overpotential (Figure S10). The O_2 detected after applying the onset potential is considerably higher than that attained by polar-

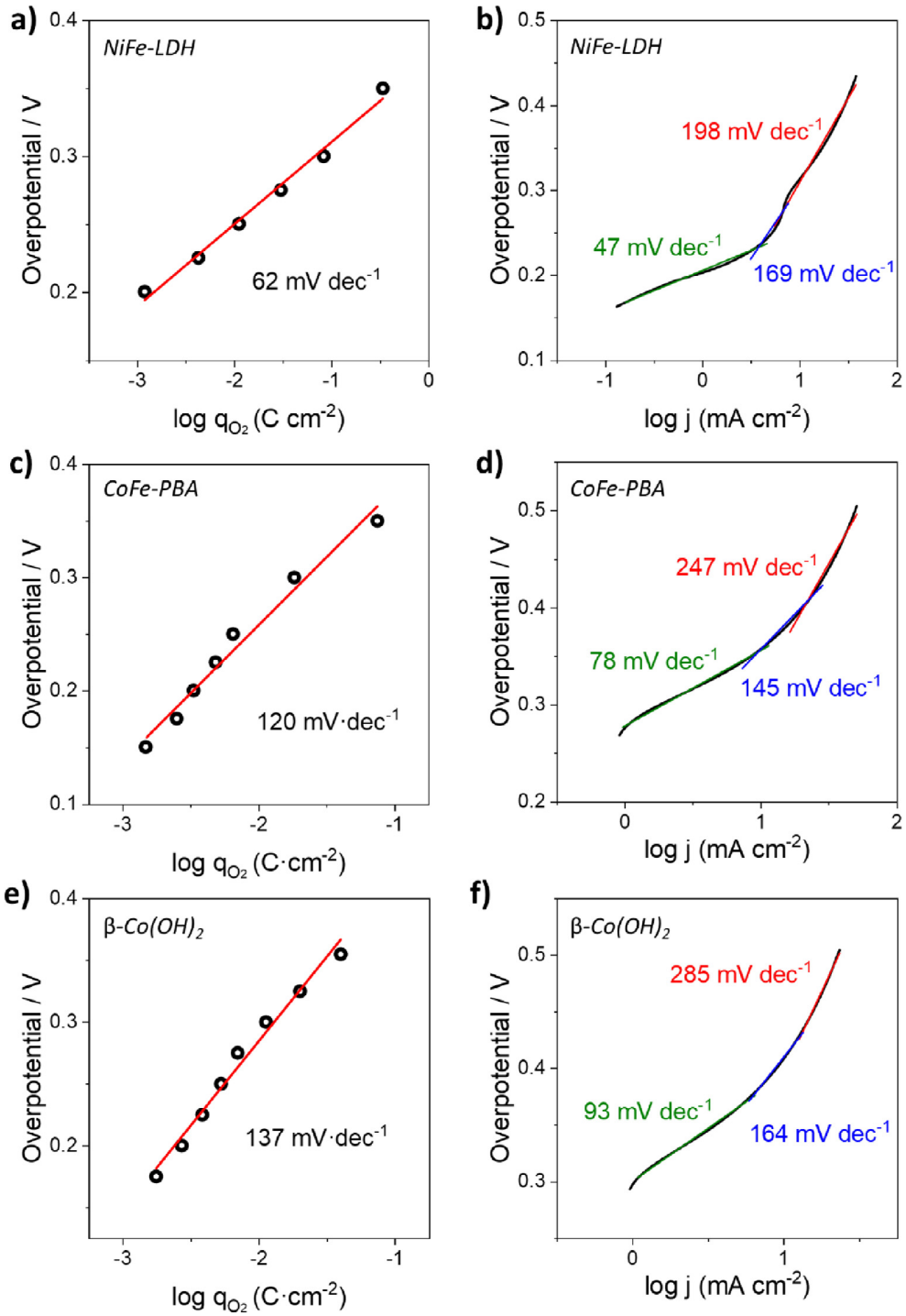

Fig. 3. Tafel slopes of the different samples obtained using irreversible charges calculated from coulovoltammograms (left axis Fig. 2) and obtained using current densities values from CVs (right axis Fig. 2). The CVs were performed at 5 mV s^{-1} in a previously N_2 purged 1 M KOH aqueous solution.

ization below the onset potential (Figure S11). In this line, at overpotentials where the O_2 production is negligible, the detected O_2 is barely the same as that attained from the blank solution, *i.e.* letting the solution 1 h without any applied voltage, which contains the O_2 coming from the air.

4. Conclusion

In summary, we have used coulovoltammetry (*i.e.* integrated voltammetry) responses at different anodic potentials in order to determine the onset potential of three different electrocatalysts (an LDH, a PBA and β-hydroxide) from the irreversible charge consumed by the Oxygen Evolution Reaction. As shown here, coulovoltammetry permits the separation, identification and quantification of the charges corresponding to reversible (electrocatalyst redox reactions) or irreversible (OER) reactions involved in electrocatalysis. Moreover, the analysis of those irreversible charges permits the calculation of the Tafel slope avoiding the parallel redox contribution of the electrocatalyst. In consequence, QV is a potential and useful technique in electrocatalysis to perform more precise quantitative studies and comparison of new earth-abundant water oxidation electrocatalysts.

Declaration of competing interest

The authors declare that they have no known competing financial interests or personal relationships that could have appeared to influence the work reported in this paper.

Acknowledgment

This work was supported by the European Research Council (ERC Starting Grant No. 2D-PnictoChem 804110 to G.A. and ERC Advanced Grant Mol-2D 788222 to E.C.), the Spanish MICINN (PID2019-111742GA-I00 to G.A., Unit of Excellence "María de Maeztu" CEX2019-000919-M, EQC2019-005816-P and project MAT2017-89993-R co-financed by FEDER) and the Generalitat Valenciana (CIDEGENT/2018/001 to G.A., Prometeo/2017/066, iDiFEDER/2018/061 and iDiFEDER/2020/063 co-financed by FEDER). R.S.-G. thanks the Ministerio de Ciencia, Innovación y Universidades, for the F.P.U. fellowship. A.S.-D thanks the Universidad de Valencia, for an 'Atracción del talento' predoctoral grant. M.C.P. thanks the Generalitat Valenciana for a postdoctoral grant. T.F.O. thanks University of Valencia for an invited Professor position.

Supplementary materials

Supplementary material associated with this article can be found, in the online version, at doi:10.1016/j.electacta.2021.138613.

References

[1] T.R. Cook, D.K. Dogutan, S.Y. Reece, Y. Surendranath, T.S. Teets, D.G. Nocera, Solar energy supply and storage for the legacy and nonlegacy worlds, Chem. Rev. 110 (2010) 6474–6502.
[2] L.Q. Zhou, C. Ling, H. Zhou, X. Wang, J. Liao, G.K. Reddy, L. Deng, T.C. Peck, R. Zhang, M.S. Whittingham, C. Wang, C.W. Chu, Y. Yao, H. Jia, A high-performance oxygen evolution catalyst in neutral-pH for sunlight-driven CO2 reduction, Nat. Commun. 10 (2019) 4081.
[3] T. Liu, J.P. Vivek, E.W. Zhao, J. Lei, N. Garcia-Araez, C.P. Grey, Current challenges and routes forward for nonaqueous lithium-air batteries, Chem. Rev. 120 (2020) 6558–6625.
[4] Z.P. Wu, X.F. Lu, S.Q. Zang, X.W. Lou, Non-noble-metal-based Electrocatalysts toward the oxygen evolution reaction, Adv. Funct. Mater. 30 (2020) 1910274.
[5] F. Lyu, Q. Wang, S.M. Choi, Y. Yin, Noble-Metal-Free electrocatalysts for oxygen evolution, Small 15 (2019) 1804201.
[6] F. Song, L. Bai, A. Moysiadou, S. Lee, C. Hu, L. Liardet, X. Hu, Transition metal oxides as electrocatalysts for the oxygen evolution reaction in alkaline solutions: an application-inspired renaissance, J. Am. Chem. Soc. 140 (2018) 7748–7759.
[7] G. Abellán, J.A. Carrasco, E. Coronado, Layered double hydroxide nanocomposites based on carbon nanoforms, in: Layer. Double Hydroxide Polym. Nanocomposites, Elsevier, 2020, pp. 411–460.
[8] M. Gong, H. Dai, A mini review of NiFe-based materials as highly active oxygen evolution reaction electrocatalysts, Nano Res. 8 (2015) 23–39.
[9] T. Wang, X. Zhang, X. Zhu, Q. Liu, S. Lu, A.M. Asiri, Y. Luo, X. Sun, Hierarchical CuO@ZnCo LDH heterostructured nanowire arrays toward enhanced water oxidation electrocatalysis, Nanoscale 12 (2020) 5359–5362.
[10] Y. Wang, T. Wang, R. Zhang, Q. Liu, Y. Luo, G. Cui, S. Lu, J. Wang, Y. Ma, X. Sun, CuO@CoFe layered double hydroxide core-shell heterostructure as an efficient water oxidation electrocatalyst under mild alkaline conditions, Inorg. Chem. 59 (2020) 9491–9495.
[11] B. Zhang, X. Zheng, O. Voznyy, R. Comin, M. Bajdich, M. García-Melchor, L. Han, J. Xu, M. Liu, L. Zheng, Homogeneously dispersed multimetal oxygen-evolving catalysts, Science 352 (2016) 333–337.
[12] D.Y. Chung, S. Park, P.P. Lopes, V.R. Stamenkovic, Y.-E. Sung, N.M. Markovic, D. Strmcnik, Electrokinetic analysis of poorly conductive electrocatalytic materials, ACS Catal. 10 (2020) 4990–4996.
[13] J.A. Carrasco, A. Harvey, D. Hanlon, V. Lloret, D. McAteer, R. Sanchis-Gual, A. Hirsch, F. Hauke, G. Abellán, J.N. Coleman, E. Coronado, Liquid phase exfoliation of carbonate-intercalated layered double hydroxides, Chem. Commun. 55 (2019) 3315–3318.
[14] D. McAteer, I.J. Godwin, Z. Ling, A. Harvey, L. He, C.S. Boland, V. Vega-Mayoral, B. Szydłowska, A.A. Rovetta, C. Backes, J.B. Boland, X. Chen, M.E.G. Lyons, J.N. Coleman, Liquid exfoliated Co(OH)2 nanosheets as low-cost, yet high-performance, catalysts for the oxygen evolution reaction, Adv. Energy Mater. 8 (2018) 1702965.
[15] G. Abellán, J.A. Carrasco, E. Coronado, J. Romero, M. Varela, Alkoxide-intercalated CoFe-layered double hydroxides as precursors of colloidal nanosheet suspensions: structural, magnetic and electrochemical properties, J. Mater. Chem. C. 2 (2014) 3723–3731.
[16] M. Ma, R. Ge, X. Ji, X. Ren, Z. Liu, A.M. Asiri, X. Sun, Benzoate anions-intercalated layered nickel hydroxide nanobelts array: an earth-abundant electrocatalyst with greatly enhanced oxygen evolution activity, ACS Sustain. Chem. Eng. 5 (2017) 9625–9629.
[17] D. Voiry, M. Chhowalla, Y. Gogotsi, N.A. Kotov, Y. Li, R.M. Penner, R.E. Schaak, P.S. Weiss, Best practices for reporting electrocatalytic performance of nanomaterials, ACS Nano 12 (2018) 9635–9638.
[18] W. Zheng, M. Liu, L.Y.S. Lee, Best practices in using foam-type electrodes for electrocatalytic performance benchmark, ACS Energy Lett 5 (2020) 3260–3264.
[19] J.G. Chen, C.W. Jones, S. Linic, V.R. Stamenkovic, Best practices in pursuit of topics in heterogeneous electrocatalysis, ACS Catal 7 (2017) 6392–6393.
[20] C. Wei, R.R. Rao, J. Peng, B. Huang, I.E.L. Stephens, M. Risch, Z.J. Xu, Y. Shao-Horn, Recommended practices and benchmark activity for hydrogen and oxygen electrocatalysis in water splitting and fuel cells, Adv. Mater. 31 (2019) 1806296.
[21] C.C.L. Mccrory, S. Jung, I.M. Ferrer, S.M. Chatman, J.C. Peters, T.F. Jaramillo, Benchmarking hydrogen evolving reaction and oxygen evolving reaction electrocatalysts for solar water splitting devices, J. Am. Chem. Soc. 137 (2015) 4347–4357.
[22] M.B. Stevens, L.J. Enman, A.S. Batchellor, M.R. Cosby, A.E. Vise, C.D.M. Trang, S.W. Boettcher, Measurement techniques for the study of thin film heterogeneous water oxidation electrocatalysts, Chem. Mater. 29 (2017) 120–140.
[23] F. Dionigi, Z. Zeng, I. Sinev, T. Merzdorf, S. Deshpande, M.B. Lopez, S. Kunze, I. Zegkinoglou, H. Sarodnik, D. Fan, A. Bergmann, J. Drnec, J.F. de Araujo, M. Gliech, D. Teschner, J. Zhu, W.X. Li, J. Greeley, B.R. Cuenya, P. Strasser, In-situ structure and catalytic mechanism of NiFe and CoFe layered double hydroxides during oxygen evolution, Nat. Commun. 11 (2020) 2522.
[24] M. Hong, C. Yang, R.A. Wong, A. Nakao, H.C. Choi, H.R. Byon, Determining the facile routes for oxygen evolution reaction by in situ probing of Li-O2 Cells with conformal Li2O2 films, J. Am. Chem. Soc. 140 (2018) 6190–6193.
[25] K. Zhu, X. Zhu, W. Yang, Application of In Situ techniques for the characterization of NiFe-based oxygen evolution reaction (OER) electrocatalysts, Angew. Chemie - Int. Ed. 58 (2019) 1252–1265.
[26] F. Dionigi, P. Strasser, NiFe-based (Oxy) hydroxide catalysts for oxygen evolution reaction in non-acidic electrolytes, Adv. Energy Mater. 6 (2016) 1600621.
[27] L.M. Cao, D. Lu, D.C. Zhong, T.B. Lu, Prussian blue analogues and their derived nanomaterials for electrocatalytic water splitting, Coord. Chem. Rev. 407 (2020) 213156.
[28] J.A. Carrasco, R. Sanchis-Gual, A.S.-D. Silva, G. Abellán, E. Coronado, A. Seijas-Da Silva, G. Abellan, E. Coronado, Influence of the interlayer space on the water oxidation performance in a family of surfactant-intercalated NiFe-layered double hydroxides, Chem. Mater. 31 (2019) 6798–6807.
[29] Z. Liu, R. Ma, M. Osada, K. Takada, T. Sasaki, Selective and controlled synthesis of α-and β-cobalt hydroxides in highly developed hexagonal platelets, J. Am. Chem. Soc. 127 (2005) 13869–13874.
[30] T.F. Otero, Coulovoltammetric and Dynamovoltammetric responses from conducting polymers and bilayer muscles as tools to identify reaction-driven structural changes. a review, Electrochim. Acta. 212 (2016) 440–457.
[31] T.F. Otero, M. Alfaro, V. Martinez, M.A. Perez, J.G. Martinez, Biomimetic structural electrochemistry from conducting polymers: Processes, charges, and energies. Coulovoltammetric results from films on metals revisited, Adv. Funct. Mater. 23 (2013) 3929–3940.
[32] L. Han, P. Tang, Á. Reyes-Carmona, B. Rodríguez-García, M. Torréns, J.R. Morante, J. Arbiol, J.R. Galan-Mascaros, Enhanced activity and acid pH stability of prussian blue-type oxygen evolution electrocatalysts processed by chemical etching, J. Am. Chem. Soc. 138 (2016) 16037–16045.
[33] J.A. Carrasco, J. Romero, M. Varela, F. Hauke, G. Abellán, A. Hirsch, E. Coronado, Alkoxide-intercalated NiFe-layered double hydroxides magnetic nanosheets as efficient water oxidation electrocatalysts, Inorg. Chem. Front. 3 (2016) 478–487.
[34] S. Pintado, S. Goberna-Ferrón, E.C. Escudero-Adán, J.R. Galán-Mascarós, Fast and persistent electrocatalytic water oxidation by Co-Fe Prussian blue coordination polymers, J. Am. Chem. Soc. 135 (2013) 13270–13273.
[35] T. Shinagawa, A.T. Garcia-Esparza, K. Takanabe, Insight on Tafel slopes from a microkinetic analysis of aqueous electrocatalysis for energy conversion, Sci. Rep. 5 (2015) 13801.
[36] Q. Zhang, N. Liu, J. Guan, Charge-transfer effects in Fe–Co and Fe–Co–Y oxides for electrocatalytic water oxidation reaction, ACS Appl. Energy Mater. 2 (2019) 8903–8911.
[37] Y. Fang, X. Li, Y. Hu, F. Li, X. Lin, M. Tian, X. An, Y. Fu, J. Jin, J. Ma, Ultrasonication-assisted ultrafast preparation of multiwalled carbon nanotubes/Au/Co3O4 tubular hybrids as superior anode materials for oxygen evolution reaction, J. Power Sources. 300 (2015) 285–293.
[38] F. Song, X. Hu, Exfoliation of layered double hydroxides for enhanced oxygen evolution catalysis, Nat. Commun. 5 (2014) 4477.
[39] Y. Zhao, X. Zhang, X. Jia, I.N. Geoffrey, R. Shi, X. Zhang, F. Zhan, Y. Tao, Sub-3 nm ultrafine monolayer layered double hydroxide nanosheets for electrochemical water oxidation, Adv. Energy Mater. (2018) 1703585.
[40] J. Zhang, J. Liu, L. Xi, Y. Yu, N. Chen, S. Sun, W. Wang, K.M. Lange, B. Zhang, Single-atom Au/NiFe layered double hydroxide electrocatalyst: probing the origin of activity for oxygen evolution reaction, J. Am. Chem. Soc. 140 (2018) 3876–3879.
[41] C.-H. Chuang, L.-Y. Hsiao, M.-H. Yeh, Y.-C. Wang, S.-C. Chang, L.-D. Tsai, K.-C. Ho, Prussian blue analogue-derived metal oxides as electrocatalysts for oxygen evolution reaction: tailoring the molar ratio of cobalt to iron, ACS Appl. Energy Mater. 3 (2020) 11752–11762.
[42] L.W. Winkler, Die bestimmung des im wasser gelösten sauerstoffes, Berichte Der Dtsch. Chem. Gesellschaft. 21 (1888) 2843–2854.